mater.scichina.com link.springer.com

Published online 13 September 2023 | https://doi.org/10.1007/s40843-023-2558-7
Sci China Mater 2023, 66(10): 3912–3921

Superior reactivity of heterogeneous single-cluster catalysts for semi-hydrogenation of acetylene

Shu Zhao[1,2], Yan Tang[3], Xiaohu Yu[4*] and Jun Li[3,5*]

ABSTRACT **Acetylene semi-hydrogenation is a vital process where the utilization of supported isolated Pd atoms as catalytic active sites is promising due to their unique reactivity and metal atom efficacy. In particular, doping Pd single atoms at different sites on metal-oxide surfaces provides an opportunity to regulate their local coordination environments and modulate their electronic and catalytic properties. In this study, we conduct extensive density functional theory calculations to investigate the influence of single Pd atom coordination environments and surface properties on the activity and selectivity of Pd_1/TiO_2 catalysts for acetylene semi-hydrogenation. Considering the activity and selectivity, a four-atom single-cluster catalyst (SCC) of Pd_1Ti_3/TiO_2 with negatively charged $Pd^{\delta-}$ sites is found to exhibit excellent catalytic performance. Moreover, both activity and selectivity are highly correlated with the surface properties, including the d-band center index and surface work function. Our work provides theoretical guidance for the future design of heterogeneous SCC on reducible oxide supports for similar reactions in heterogeneous catalysis.**

Keywords: acetylene, semi-hydrogenation, single-cluster catalysts (SCCs), TiO_2, DFT

INTRODUCTION

Semi-hydrogenation of acetylene in ethylene-rich streams is an industrially important process. This reaction is used to remove trace amounts of acetylene impurities in the feedstock for industrial ethylene polymerization to produce polyethylene [1]. The undesired acetylene content has to be removed from usually 0.1–1 vol% to lower than 5 ppm range, which would otherwise poison the downstream polymerization catalyst [2–4]. The hydrogenation catalysts are required to be effectively and selectively converting C–C triple bonds to double bonds, but not further to single ones. Therefore, how to understand the selectivity of semi-hydrogenation catalysts is scientifically attractive and designing new semi-hydrogenation catalysts with high selectivity is critical in industrial applications [5,6].

Palladium-based catalysts are commonly known for their excellent selectivity and widespread application in the semi-hydrogenation of acetylene. Extensive research has been conducted to regulate the electronic and geometric structure of active clusters in order to suppress the over-hydrogenation of acetylene [6–9]. Among these efforts, the strategy of improving the isolation of active sites has garnered increasing interest to enhance the selectivity of hydrogenation products and achieve high metal atom efficacy. The forefront of this attempt is the development of single-atom catalysts (SACs) [10–13], which have been used successfully in hydrogenation reactions [14–22], oxidation reactions [10,23–29] and water-gas shift (WGS) reaction [30–33], etc. Zheng's group [15] provided a room-temperature photochemical strategy to produce atomically dispersed Pd catalysts, and found that the Pd_1/TiO_2 catalysts exhibit extremely high catalytic activity and stability in hydrogenation of C=C and C=O bonds. Lu's group [16] found that a Pd_1/graphene catalyst showed high selectivity of nearly 100% to butenes in the selective hydrogenation of 1,3-butadiene, with a conversion rate of 95%. Vilé *et al.* [20] carried out a joint experimental and theoretical study to propose that the high catalytic performance of the Pd_1/C_3N_4 system for the hydrogenation of alkynes was related to the favorable hydrogen activation and adsorption of alkynes on the atomically dispersed Pd sites. The intermetallic compounds with single-atom Pd sites achieved the high ethylene selectivity for semi-hydrogenation of acetylene [17,34,35].

Density functional theory (DFT) calculations demonstrated that the weak π-bonding for ethylene adsorption on the single-atom Pd sites suppresses its further hydrogenation, while the σ-bonding for acetylene adsorption facilitates its hydrogenation. Some other single-atom alloy catalysts [36] also have high acetylene conversion and high selectivity to ethylene, such as Pd-Ag [36], Pd-Au [37] and Pt-Cu [38] alloys at the single-atom limit. Recently, the singly dispersed bimetallic Rh_1Co_3 sites on CoO surface were identified to exhibit distinctly different catalytic performance in reduction of NO with CO and N_2-to-NH_3 thermal conversion [39–41]. The well-dispersed surface-anchored metal clusters form a new type of catalysts named heterogeneous single-cluster catalyst (SCC) [42–49]. The graphdiyne-supported SCCs also have shown high selectivity for a series of reactions, including semi-hydrogenation of acetylene [43]. Therefore, the SCCs open up more opportunities to

[1] Institute of Advanced Battery Materials and Devices, Faculty of Materials and Manufacturing, Beijing University of Technology, Beijing 100124, China
[2] Key Laboratory of Advanced Functional Materials, Ministry of Education, Beijing University of Technology, Beijing 100124, China
[3] Department of Chemistry and Engineering Research Center of Advanced Rare-Earth Materials of Ministry of Education, Tsinghua University, Beijing 100084, China
[4] Shaanxi Key Laboratory of Catalysis, School of Chemical & Environment Sciences, Shaanxi University of Technology, Hanzhong 723000, China
[5] Department of Chemistry, Southern University of Science and Technology, Shenzhen 518055, China
Corresponding authors (emails: yuxiaohu@snut.edu.cn (Yu X); junli@tsinghua.edu.cn (Li J))

improve selectivity in hydrogenation reactions, and the atomic-level understanding of this process is extremely important.

TiO_2 is commonly used as a support for the acetylene hydrogenation because of the role of reducible oxide support in the strong metal-support interaction phenomenon. The interaction between the oxide support and the metal particles is believed to have a significant impact on the catalyst activity and selectivity of the hydrogenation reaction [50,51]. Kim [52] found that TiO_2-supported Pd catalysts have high ethylene selectivity for acetylene hydrogenation. Panpranot *et al.* [53] prepared Pd/TiO_2 catalysts and clarified that the Ti^{3+} in contact with Pd can probably reduce the adsorption strength of ethylene, thereby increasing the selectivity of ethylene. Yang *et al.* [54] investigated the reaction mechanism of selective hydrogenation of acetylene on Pd_4 clusters supported on anatase TiO_2 (101) and rutile TiO_2 (110), and found that the anatase TiO_2 catalyst has higher selectivity of acetylene hydrogenation than the rutile one. Recently, Yang *et al.* [22] found that Pd_1/TiO_2 has superior activity and selectivity in the selective semi-hydrogenation of phenylacetylene compared with commercial catalysts. In addition, it is also reported that Pd_1/TiO_2 catalyst can facilitate the activation of O_2 into superoxide (O_2^-) to promote the catalytic oxidation [55] and analyze the organophosphorus pesticide chlorpyrifos as a photocatalytic sensing platform [56], and so on.

Therefore, the utilization of TiO_2-supported isolated Pd atoms as catalytic active sites for acetylene semi-hydrogenation has garnered significant interest due to their distinct reactivity and efficient metal utilization. However, the relationship between the local coordination environment of Pd single atoms on the TiO_2 surface and their catalytic activity and selectivity is yet to be understood. Thus, the main focus of this study is to elucidate the local structural and electronic properties of single Pd atoms located at different sites on the TiO_2 (101) surface, as well as to investigate the reaction mechanism and catalytic behavior for semi-hydrogenation of acetylene on these Pd_1/TiO_2 catalysts. The insights gained from these analyses can provide a theoretical foundation for the design of new SACs and SCCs for the semi-hydrogenation of acetylene.

EXPERIMENTAL SECTION

All the calculations were carried out with Vienna *ab initio* simulation package (VASP) using spin-polarized DFT methods [57,58]. The projector augmented wave (PAW) method was chosen to describe the interactions between ions and valence electrons [59,60], and the exchange-correlation interaction of valence electrons was calculated by generalized gradient approximation in the Perdew–Burke–Ernzerhof form (GGA-PBE) [61]. The valence orbitals of Pd (4d, 5s), Ti (3d, 4s), O (2s, 2p), C (2s, 2p) and H (1s) were described by plane-wave basis sets with cutoff energies of 400 eV. The DFT + U approach was applied to the calculation of the electronic structure of TiO_2, and the Hubbard parameters were set to $U - J = 4$ eV for Ti [62]. The Monkhorst-Pack ($2 \times 2 \times 1$) k-point grid sampling within Brillouin zones was used. The convergence criterium of the electronic self-consistent iteration was set to 10^{-4} eV, and the residual force was set below 0.03 eV Å^{-1}. The transition states (TSs) were searched using the improved dimer method [63] and the climbing image nudged elastic band (CI-NEB) method [64,65]. The electron density differences were evaluated using the formula $\Delta\rho = \rho(Pd_1/substrate) - \rho(Pd_1) - \rho(substrate)$. Atomic charges were computed using the atom-in-molecule (AIM) scheme proposed by Bader [66,67]. Crystal orbital Hamilton population (COHP) analysis was performed by using LOBSTER package [68,69].

In this work, the calculated bulk lattice parameters of anatase TiO_2 (a = 3.86 Å, c = 9.50 Å) are in agreement with the experimental data (a = 3.78 Å, c = 9.51 Å) [70]. For modeling TiO_2 (101) surface, the $p(2 \times 3)$ slab containing four layers of Ti atoms and eight layers of O atoms was used as shown in Fig. 1. In the calculations, the bottom five layers were fixed in their bulk position during geometry optimization. The vacuum layers were set to 15 Å for all supercells to avoid artificial interaction between the images. The adsorption energy of adsorbate was defined as $E_{ads} = E(adsorbate/substrate) - E(substrate) + E(adsorbate)$, in which $E(adsorbate/substrate)$, $E(adsorbate)$, and $E(substrate)$ are the calculated total energies of a substrate with the adsorbate, a gaseous-phase molecule (adsorbate), and a clean substrate, respectively. Based on the calculated harmonic vibrational frequencies, the zero-point vibration energies (ZPE) were evaluated and added in the electronic total energies.

RESULTS AND DISCUSSION

Surface model

It is well known that TiO_2 (101) surface is the most stable and frequently exposed surface of anatase [71]. As shown in Fig. 1, the (101) surface presents a stepped structure, and has under-coordinated five-fold Ti (Ti_{5c}) and two-fold O (O_{2c}) atoms, as well as fully coordinated Ti_{6c} and two types of O_{3c} sites.

Experimentally, the precise synthesis of single atoms on the TiO_2 surface at different sites can be achieved through suitable preparation methods. For example, single atoms can be loaded onto the surface of a support material or doped at oxygen or metal defects [15,22,56,72–75]. Therefore, in order to explore the various potential configurations of a single Pd atom on the TiO_2 (101) surface, we have positioned the single-atom Pd at four different locations, as illustrated in Fig. 2. Fig. 2a, b show that the single-atom Pd substitutes an O_{2c} and an O_{3c} atom, respectively. In both cases, the anchored Pd atom is bonded to the Ti atoms, thus forming the Pd_1Ti_2 and Pd_1Ti_3 SCCs. The Pd atoms in both bimetallic positions obtain electrons from the lattice and form negatively charged $Pd^{\delta-}$ ions (Table 1 and Fig. 2a, b). As presented in the projected density of state (PDOS, Fig. 3a, b), both 5s and 4d orbitals of Pd in Pd_1Ti_2 and Pd_1Ti_3 are found below Fermi level, respectively, indicating the formation of $Pd^{\delta-}$ anion. According to the binding energy, the Pd atom at Pd_1Ti_3 site is slightly more stable than the Pd atom at Pd_1Ti_2 site. Fig. 2c shows that the single-atom Pd substitutes a Ti_{5c} atom (Pd_{Ti} model), in which case the anchored Pd atom is bonded to five

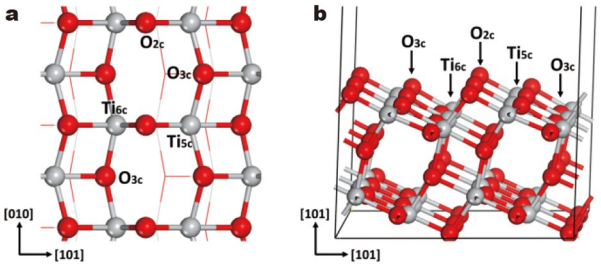

Figure 1 (a) Top and (b) side views of anatase TiO_2 (101) supercell (O: red, Ti: gray).

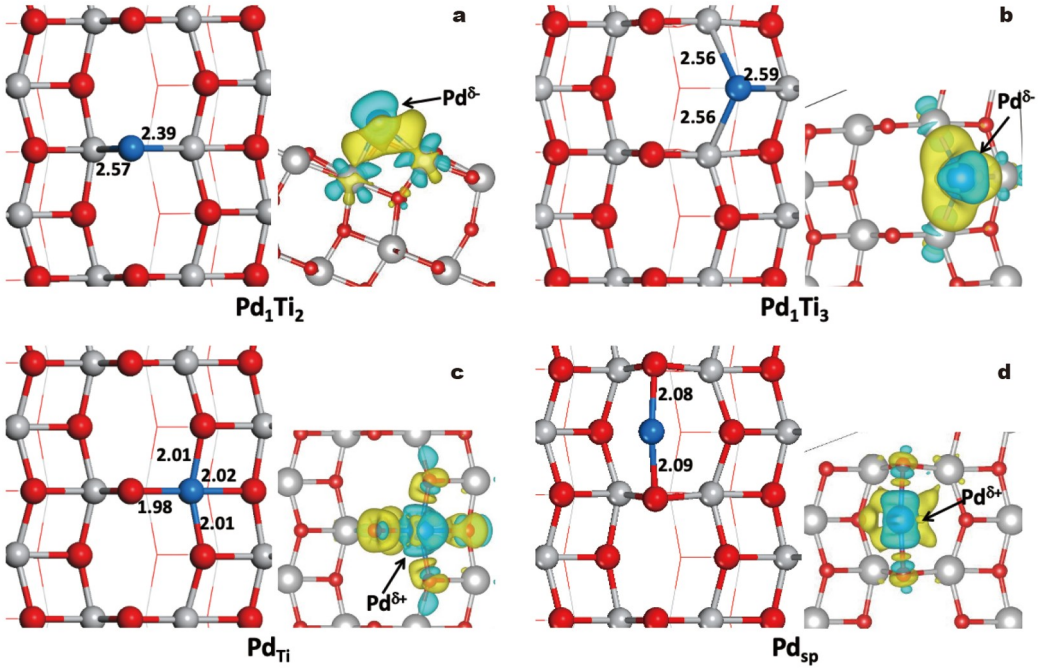

Figure 2 Optimized structures and calculated charge density differences for (a) Pd_1Ti_2, (b) Pd_1Ti_3, (c) Pd_{Ti} and (d) Pd_{sp} model configurations (O: red, Ti: gray, Pd: blue; the bond length in Å). Blue and yellow areas represent charge reduction and increase, respectively. The cutoff of the density-difference isosurfaces is equal to 0.004 electrons $Å^{-3}$.

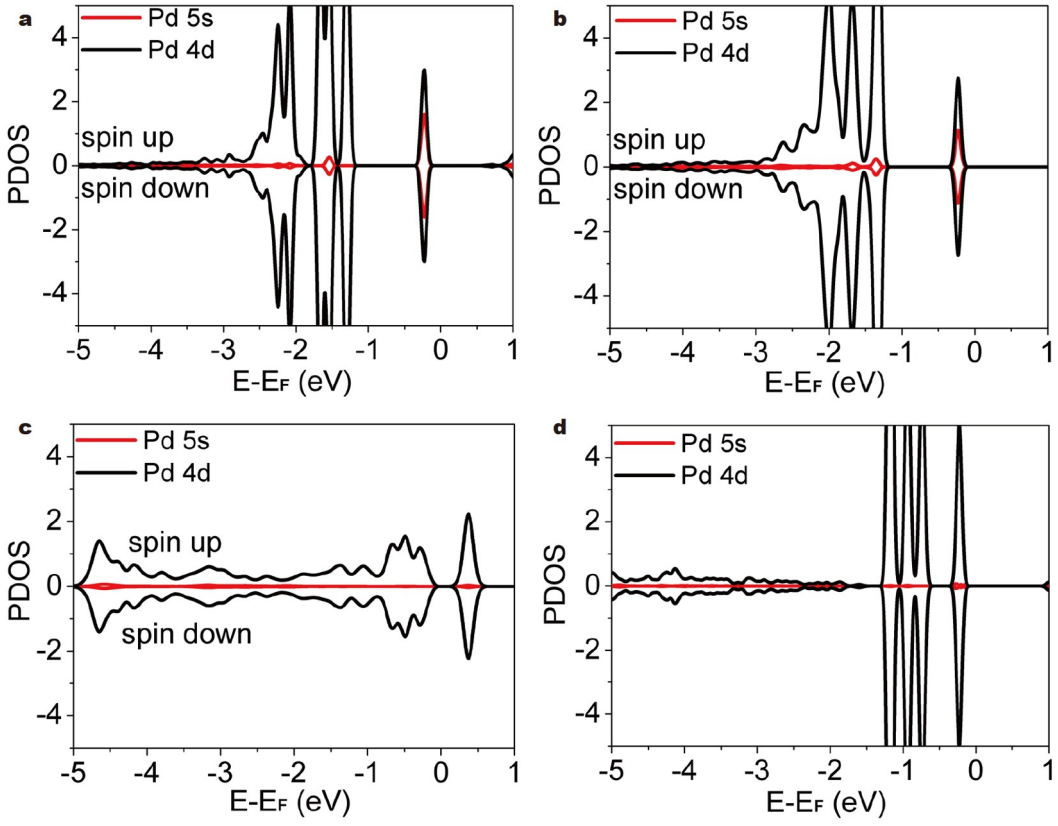

Figure 3 PDOS of Pd atoms in the (a) Pd_1Ti_2, (b) Pd_1Ti_3, (c) Pd_{Ti}/TiO_2 and (d) Pd_{sp} models. Energies are referred to the Fermi level.

oxygen atoms with a positive charge of +1.52 |e| according to Bader charge analysis. The PDOS of Pd atom (Fig. 3c and Fig. S1) illustrates that the $d_{x^2-y^2}$ orbital and a significant portion of the d_{xz} orbital of the Pd single atom are unoccupied, while a portion of the d_{z^2} orbital is observed above the Fermi Level. This observation suggests that the oxidation state of the single-atom

Pd is approximately +4. The Pd atom in the Pd_{Ti} model is found to have the strongest binding energy among these four Pd_1/TiO_2 models, indicating that the Pd substitution of Ti_{5c} on the TiO_2 (101) surface is thermodynamically quite stable. Fig. 2d shows that the single-atom Pd is located on the surface (Pd_{sp} model). The Pd adatom prefers to locate at the bridge site between two O_{2c} atoms, which is consistent with previous work [76]. The calculated adsorption energy is −2.29 eV, and Pd–O bond lengths are 2.08 and 2.09 Å, respectively. The Bader charge analysis reveals that only 0.19 |e| are transferred from the metal to the oxide surface, leading to the formation of a slightly positively charged $Pd^{\delta+}$ ion in this case. The PDOS in Fig. 3d shows that Pd adatom maintains the d^{10} electronic state because only 4d orbitals of Pd is found below Fermi level.

The COHP analysis was adopted to characterize the bonding orbitals and corresponding bonding strength. From the projected COHP analysis (Fig. 4), the Pd 4d and Ti 3d orbitals as well as Pd 4d and O 2p orbitals result in the bonding contributions below the Fermi level and most of the antibonding interactions above the Fermi level. For the Pd_1Ti_2 model (Fig. 4a), the bonding contribution mainly comes from d_{xz} and d_{z^2} orbitals of Pd with the d_{xz} orbitals of two Ti atoms. For the Pd_1Ti_3 model (Fig. 4b), the bonding is mainly caused by the d_{xz} and d_{yz} orbitals of Pd and the d orbitals of the three Ti atoms. As

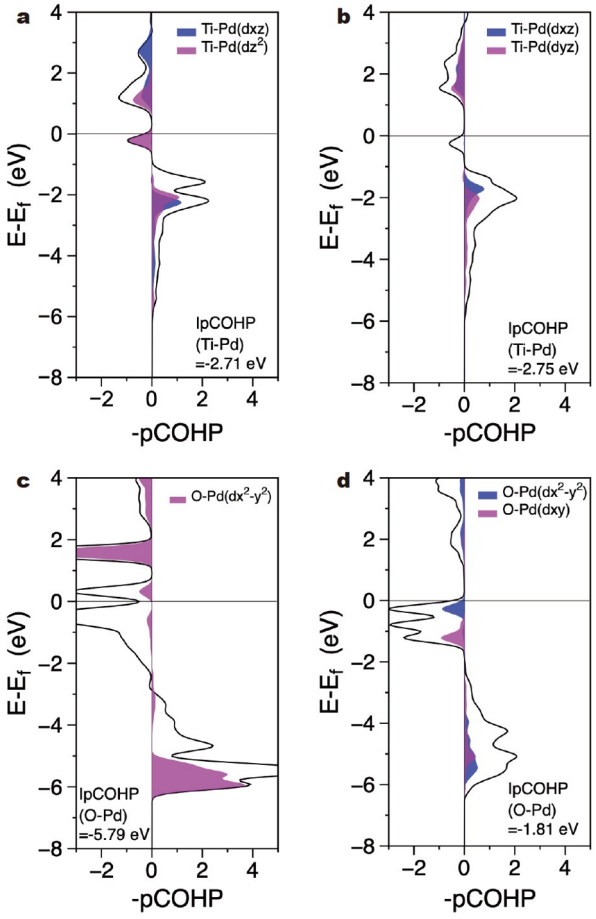

Figure 4 pCOHP between the metal center from Pd to Ti and O atoms on (a) Pd_1Ti_2, (b) Pd_1Ti_3, (c) Pd_{Ti} and (d) Pd_{sp} models and corresponding integrated values (IpCOHP). The negative value of −pCOHP represents the anti-bonding state, while the positive value of −pCOHP represents the bonding state.

presented in projected COHP (pCOHP) of Pd_{Ti} model (Fig. 4c), the splitting $d_{x^2-y^2}$ of the Pd atom interacts with 2p orbital of five O atoms that stabilizes the binding of the Pd atom. As for the Pd_{sp} model (Fig. 4d), it is mainly the d_{xy} and $d_{x^2-y^2}$ orbitals of the Pd atom and the 2p orbitals of the two O atoms that result in the bonding contribution. The integrated pCOHP (IpCOHP) can be used to quantify the bonding strength [77]. As presented in Fig. 4, the IpCOHP summed over all ligands of each Pd atom are −5.79, −2.75 and −2.71 eV in Pd_{Ti}, Pd_1Ti_3 and Pd_1Ti_2 models, respectively. However, the IpCOHP of the Pd atom in Pd_{sp} model is only −1.81 eV, indicating that the bonding of the supported Pd atom is weaker than the bonding of the substituted Pd atom, which is consistent with the binding energy of single-atom Pd at different sites (Table 1).

Adsorption properties of possible C_2H_x species on Pd_1/TiO_2

The adsorptions energies of C_2H_2, C_2H_3, C_2H_4 and C_2H_5 species on the four Pd_1/TiO_2 models were firstly calculated to obtain the most stable configurations. The adsorption energies are presented in Fig. 5 and Table S1, the corresponding optimized structures are shown in Fig. S2. On these four Pd_1/TiO_2 surfaces, the adsorption energies of acetylene and ethylene follow the order of Pd_1Ti_2 < Pd_{Ti} < Pd_1Ti_3 < Pd_{sp}. Both C_2H_2 and C_2H_4 favor the π adsorption mode in which two carbon atoms are bonded to the single-atom Pd. Due to the activation effect of Pd, the C–C bond length of the C_2H_x species on the Pd_1/TiO_2 catalysts becomes longer than that of the gas-phase species. Among these four surfaces, Pd_{sp} model has the greatest C_2H_4 adsorption energy of −1.53 eV, indicating that ethylene is not conducive to desorption and may lead to the formation of undesired ethane. The most stable adsorption site for H is located on the O_{2c} atom next to the Pd atom. The adsorption energy of H atoms shows a linear relationship with the Bader charge of the O atom on the different Pd_1/TiO_2 models (Fig. S3). Specifically, the adsorption energy of H on Pd_{Ti} (−2.14 eV) is significantly higher compared with the other three models. This is because in the Pd_{Ti} model, the O atom connected to Pd has the least negative charge, making it more prone to electron uptake from H and thus exhibit the strongest H adsorption capability.

C_2H_2 hydrogenation mechanism

C_2H_2 hydrogenation on Pd_1Ti_2 model

The potential energy profile of C_2H_2 hydrogenation on the Pd_1Ti_2 model is shown by the black line in Fig. 6a, and the configurations of the TSs are shown in Fig. S4. The hydrogenation barriers (E_a), reaction energies (E_r) and the C–H distances at the TSs are summarized in Table S2. On the Pd_1Ti_2 model, C_2H_2 is adsorbed on the single-atom Pd with an

Table 1 Bader charges and binding energies of single-atom Pd at different sites[a]

	Pd_1Ti_2	Pd_1Ti_3	Pd_{Ti}	Pd_{sp}
Bader charge (Pd) (|e|)	−0.74	−0.82	+1.52	+0.19
Binding energy (Pd) (eV)	−2.77	−3.20	−3.53	−2.29

a) The formation energy of Pd substituted surface (Pd_{Ti}) was calculated using the equation: $Pd(s) + Ti_xO_{2x}(surf) + O_2(g) \rightarrow PdTi_{x-1}O_{2x}(surf) + TiO_2(s)$.

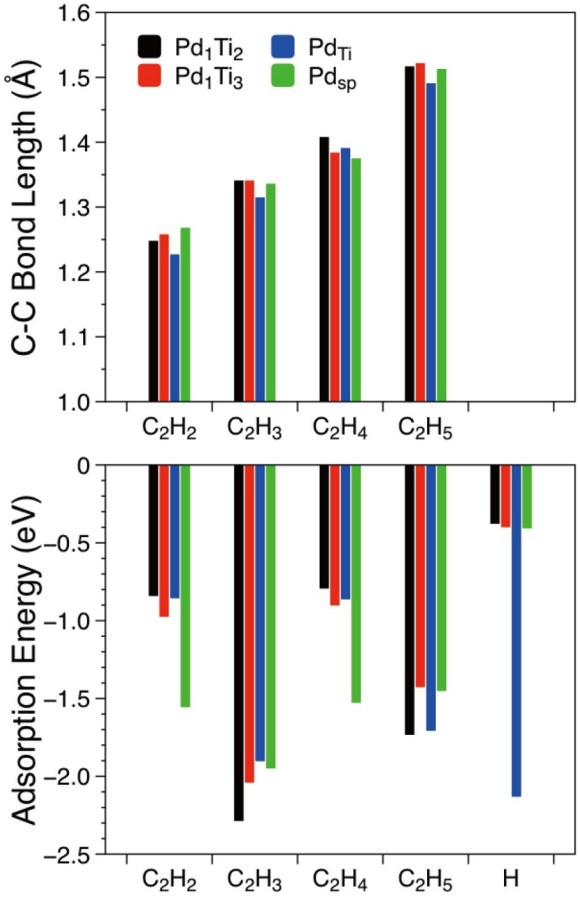

Figure 5 C–C bond lengths and adsorption energies of C_2H_x and H on Pd_1/TiO_2 surfaces.

adsorption energy of −0.85 eV, which is conductive to hydrogenation to C_2H_4 through the ethylene-like C_2H_3Pd intermediate (Fig. S2). C_2H_4 also locates on the single Pd atom through a weak π bond, and the adsorption energy is −0.80 eV. It is found that the first hydrogenation step, $C_2H_2^* + H^* \rightarrow C_2H_3^*$, has the lowest activation barrier (0.44 eV) in the entire pathway and exothermic by 0.81 eV. The barriers of the next two steps are slightly higher, 1.19 eV for TS2 and 1.27 eV for TS3, and the reactions are exothermic by 0.28 and 0.13 eV, respectively. The desorption energy of C_2H_4 on Pd_1Ti_2 model is 0.80 eV, smaller than its further hydrogenation barrier (1.27 eV). And the transition-state energy of C_2H_4 hydrogenation (TS3) is higher than the energy of gas-phase ethylene (the black dotted line in Fig. 6a), which indicates that the ethylene is more prone to desorption in the subsequent process without further hydrogenation.

Since the temperature has a significant effect on the adsorption and desorption processes when entropy plays a significant role, we considered the entropic effects from gas phase acetylene and hydrogen to the gas phase ethane under standard pressure. The influence of the entropy is in the form of chemical potential, which can be obtained using the following equation:

$$\mu_i(T, p_i) = E_i(0\ \mathrm{K}) + \tilde{\mu}_i(T, p^\theta) + k_B T \ln\left(\frac{p_i}{p^\theta}\right).$$

$E_i(0\ \mathrm{K})$ is the DFT energy of the ideal gas molecule including zero-point energy; $\tilde{\mu}_i(T, p^\theta)$ includes the thermal contribution of ideal gas molecule and the entropy of ideal gas molecule at 1 atm (1 atm = 1.01×10^5 Pa), which are given in the Supplementary information (Table S3). With the increase of temperature, the desorption of ethylene becomes much easier. At 400 K, the energy of adsorbed C_2H_4 is higher than that of gas-phase ethylene (the blue dashed line in Fig. 6a), suggesting the ethylene molecule desorbs from the surface spontaneously. Hence, Pd_1Ti_2 SCC exhibits high selectivity in the semi-hydrogenation reaction of acetylene. When the temperature increases to 500 K (the green line in Fig. 6a), the adsorption of acetylene and hydrogen becomes unfavorable. Thus, entropic effects at 400 K are considered in the following discussion.

C_2H_2 hydrogenation on Pd_1Ti_3 model

The potential energy profile of acetylene hydrogenation on Pd_1Ti_3 SCC at 400 K is shown as the blue line in Fig. 6b, and the configurations of the TSs are shown in Fig. S4. The barriers of C_2H_2 and C_2H_3 hydrogenation are 0.62 and 0.91 eV, and these two steps are highly exothermic by 0.67 and 1.00 eV, respectively (Table S2). The rate-limiting step of the entire process on Pd_1Ti_3 SCC is the hydrogenation of C_2H_4, i.e., $C_2H_4^* + H^* \rightarrow C_2H_5^*$, with a barrier of 1.33 eV and endothermicity of 0.42 eV. It is clear that the energy of $C_2H_4^*$ is very close to the energy of gas-phase ethylene at 400 K, and the hydrogenation barrier of C_2H_4

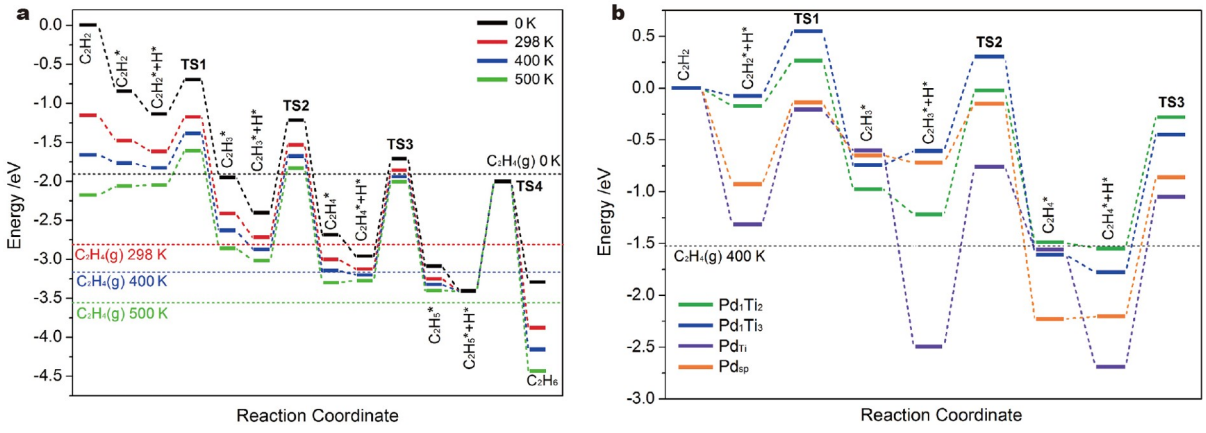

Figure 6 (a) Step-by-step hydrogenation mechanism of acetylene to ethane on the Pd_1Ti_2 model at different temperatures. (b) Potential energy profiles of C_2H_2 hydrogenation at 400 K on Pd_1/TiO_2 surfaces.

is much higher than its desorption energy, indicating that ethylene does not further hydrogenate, but desorbs from the surface. There, similar to Pd_1Ti_2, Pd_1Ti_3 SCC also has good selectivity in the semi-hydrogenation of C_2H_2.

C_2H_2 hydrogenation on Pd_{Ti} model

The potential energy profile for acetylene hydrogenation on Pd_{Ti} model is shown as a purple line in Fig. 6b. As presented in Fig. 6b and Table S2, the hydrogenation of C_2H_2 to C_2H_3 has the lowest barrier in the entire hydrogenation process, with an activation energy of 1.10 eV (TS1) and endothermicity of 0.71 eV. The barrier of C_2H_3 hydrogenation is 1.74 eV (TS2) and this step is endothermic by 0.94 eV. The energy of adsorbed C_2H_4 is close to the energy of gas-phase C_2H_4 at 400 K, which is much lower than its subsequent hydrogenation barrier (TS3, 1.64 eV), suggesting that the Pd_{Ti} model will exhibit high selectivity in the semi-hydrogenation of C_2H_2. Since the H atom has a considerable adsorption energy (−2.14 eV) on the Pd atom of Pd_{Ti} model, each hydrogenation step has a high barrier and is a strong endothermic process, which leads to a low activity of C_2H_2 hydrogenation. The linear relationships between the hydrogen adsorption energies and C_2H_4 formation energies as well as hydrogenation barriers of C_2H_4 were found, as shown in Fig. S5.

C_2H_2 hydrogenation on Pd_{sp} model

The potential energy profile for C_2H_2 hydrogenation on Pd_{sp} model is shown as an orange line in Fig. 6b. Among these four Pd_1/TiO_2 models, the adsorption energy of C_2H_2 and C_2H_4 on Pd_{sp} model is the largest. The adsorption energy of C_2H_4 is −1.53 eV, indicating that the desorption of C_2H_4 is rather difficult. The barrier of the first hydrogenation step is 0.78 eV (TS1), and the reaction is slightly endothermic by 0.28 eV. The next step, $C_2H_3^* + H^* \rightarrow C_2H_4^*$, has a low barrier of 0.57 eV, and is highly exothermic by 1.51 eV, indicating that the Pd_{sp} catalyst has high activity for C_2H_2 hydrogenation. The further hydrogenation of C_2H_4 to C_2H_5 is the rate-determining step in the entire C_2H_2 hydrogenation process, with a high barrier of 1.35 eV (TS3). However, the barrier (TS3) is still lower than the desorption energy of C_2H_4, and the energy of $C_2H_4^*$ is much lower than the energy of gas-phase C_2H_4 at 400 K. Thus, C_2H_4 will be further hydrogenated before desorption from the surface, resulting in the formation of undesirable ethane.

Ethylene selectivity on Pd_1/TiO_2 surfaces

The selectivity between the semi-hydrogenation of C_2H_2 to C_2H_4 and the further hydrogenation to C_2H_6 reaction depends on the adsorption energy of C_2H_4 and the reaction barrier for its further hydrogenation (Fig. 7a). A lower adsorption energy of C_2H_4 and a higher barrier for its further hydrogenation suggest that C_2H_4 is more likely to desorb from the surface rather than undergo excessive hydrogenation. In this scenario, the catalyst demonstrates a higher selectivity towards C_2H_4 formation. To quantitatively estimate the selectivity, we define $\Delta E = E_a - |E_{ads}|$ as the difference between the hydrogenation barrier of C_2H_4 (E_a) and the absolute value of the adsorption energy of C_2H_4 ($|E_{ads}|$) on these surfaces [78,79]. As indicated in Table S4, all catalysts, except for Pd_{sp}, exhibit positive ΔE values. A positive ΔE value

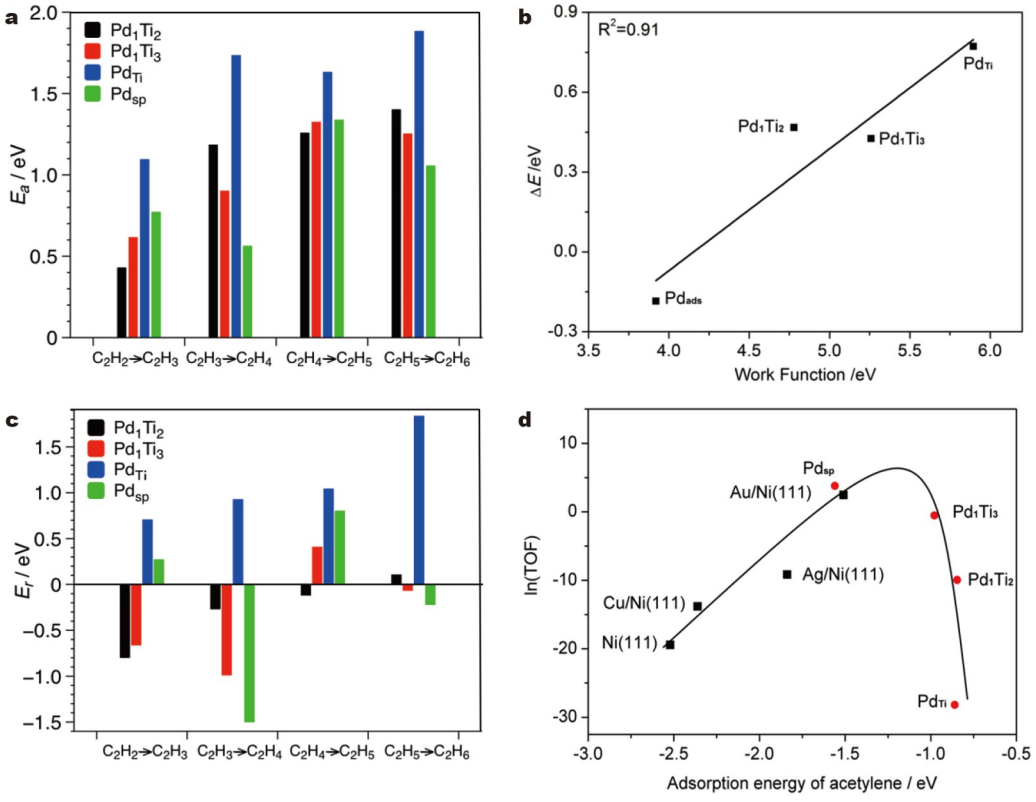

Figure 7 (a) Activation barriers for the hydrogenation of C_2H_2 on Pd_1/TiO_2 surfaces. (b) Relationship between ΔE and work function of Pd_1/TiO_2 surfaces. (c) Reaction energies for the hydrogenation of C_2H_2 on Pd_1/TiO_2 surfaces. (d) Volcano type of curve in which ln(TOF) is plotted as a function of the adsorption energies of C_2H_2 (the black squares represent the data referenced from Ref. [78]).

signifies a preference for C_2H_4 desorption over further hydrogenation, with larger ΔE values corresponding to higher selectivity. Therefore, the selectivity of these four systems can be ranked as follows: $Pd_{Ti} > Pd_1Ti_3 \approx Pd_1Ti_2 > Pd_{sp}$. More importantly, a linear relationship is found between the ΔE and surface work function (Fig. 7b). On the basis of these correlations, one can both predict the reactivity for C_2H_4 formation on various surfaces *via* analyzing their surface properties and deduce the different dopants that can increase the C_2H_4 selectivity in semi-hydrogenation of C_2H_2.

Activity of C_2H_2 hydrogenation on Pd_1/TiO_2 surfaces

In addition to selectivity, the different activities of acetylene hydrogenation on the four Pd_1/TiO_2 models are also compared from both thermodynamic and kinetic perspectives. Thermodynamically, the reactivity of forming C_2H_4 on the Pd_1/TiO_2 surfaces can be described by the reaction energy of each hydrogenation step. As presented in Fig. 7c, each step of hydrogenation of C_2H_2 on the Pd_1Ti_2 model is an exothermic process. Similarly, in addition to the hydrogenation of C_2H_4, each hydrogenation step of C_2H_2 on the Pd_1Ti_3 model is exothermic. On the Pd_{sp} model, the elementary step $C_2H_3^* + H^* \rightarrow C_2H_4^*$ is the most exothermic reaction, while the hydrogenation of C_2H_2 and C_2H_4 is an endothermic process. The C_2H_2 hydrogenation on the Pd_{Ti} model is a thermodynamically unfavorable process, and each step is a strongly endothermic process. Furthermore, a linear relationship was found between the reaction energy of the entire reaction ($C_2H_2^* + H_2 \rightarrow C_2H_4^*$) and the d-band center index [80] of the single-atom Pd in the four systems (Fig. S6), indicating that the reaction energy increases with the increase of the d-band center of these Pd_1/TiO_2 surfaces. Among these four catalysts, C_2H_4 formation on the Pd_1Ti_3 SCC is the most thermodynamically favored, followed by Pd_1Ti_2, Pd_{sp}, and Pd_{Ti}.

Kinetically, the activity of the C_2H_2 hydrogenation can be estimated as following. According to the energetic span theory, the turnover frequencies (TOF) can be written as $\mathrm{TOF} \approx \frac{k_B T}{h} e^{-E_a^{\mathrm{eff}}/RT}$, where E_a^{eff} is the effective barrier of the reaction, which is defined as the energy difference between the highest TS and the most stable intermediate species [78,81–83]. The estimated ln(TOF) was plotted against the adsorption energies of C_2H_2 on the Pd_1/TiO_2 surfaces as shown in Fig. 7d. Hu's group [78] investigated the activity of C_2H_4 formation on Ni surfaces doped by Au, Ag, and Cu. They found the most inert dopant Au on the Ni surface weakens the C_2H_2 adsorption and gives the highest activity. As can be seen from Fig. 7d, Pd_{sp} and Ni catalysts are located on the strongly adsorbed side of the volcano curve, while Pd_1Ti_2, Pd_1Ti_3, and Pd_{Ti} catalysts are located on the weakly adsorbed side. Among these systems, Pd_{sp} and Pd_1Ti_3 are the most active and very close to Au/Ni(111), followed by Pd_1Ti_2, while Pd_{Ti} is the least active. The observed difference in activity can be attributed to the variation in the adsorption energy of H atoms on the different Pd_1/TiO_2 models. In particular, the adsorption energy of H on Pd_{Ti} is significantly higher compared with the other three models. Consequently, a higher energy barrier is required to activate the H atom from its initial adsorption state to the TS, resulting in a higher hydrogenation barrier on the Pd_{Ti} model. Due to its low activity, the Pd_{Ti} model is not considered a favorable candidate for C_2H_2 semi-hydrogenation. Additionally, as previously discussed, Pd_{sp} exhibits poor selectivity for C_2H_2 semi-hydrogenation. Consequently, the Pd_1Ti_3 SCC with bimetallic sites exhibits not only the highest selectivity but also the highest activity among the four Pd_1/TiO_2 models when considering both thermodynamic and kinetic perspectives.

CONCLUSIONS

In this work, in order to reveal the underlying influence of single-atom Pd location and surface properties on the reaction performance, extensive DFT calculations are performed to elucidate the activity and selectivity of acetylene hydrogenation to ethylene on several Pd_1/TiO_2 catalysts. The activity of different SACs Pd_1/TiO_2 and SCCs for semi-hydrogenation of acetylene is found to follow the order of $Pd_1Ti_3 \approx Pd_{sp} > Pd_1Ti_2 > Pd_{Ti}$. The poor activity of Pd_{Ti} model can be explained by the strong adsorption of the hydrogen atom on the surface. It is especially noteworthy that Pd_1Ti_3 and Pd_1Ti_2 SCCs have high selectivity for semi-hydrogenation of acetylene, while ethylene tends to be fully hydrogenated to ethane on Pd_{sp} model. The Pd_1Ti_3 SCC with negatively charged $Pd^{\delta-}$ bimetallic sites exhibits excellent catalytic performance both in terms of activity and selectivity among all considered Pd_1/TiO_2 catalysts. Moreover, both activity and selectivity are highly correlated with the surface properties, especially the d-band center index and surface work function. The catalyst with larger d-band center and surface work function has higher activity and selectivity. Our studies may provide a theoretical foundation for future design of highly efficient SCCs on reducible oxide supports for hydrogenation reactions in heterogeneous catalysis.

Received 27 March 2023; accepted 21 July 2023; published online 13 September 2023

1 Huang W, Mccormick J, Lobo R, *et al.* Selective hydrogenation of acetylene in the presence of ethylene on zeolite-supported bimetallic catalysts. J Catal, 2007, 246: 40–51
2 Cao X, Mirjalili A, Wheeler J, *et al.* Investigation of the preparation methodologies of Pd-Cu single atom alloy catalysts for selective hydrogenation of acetylene. Front Chem Sci Eng, 2015, 9: 442–449
3 Schbib NS, García MA, Gígola CE, *et al.* Kinetics of front-end acetylene hydrogenation in ethylene production. Ind Eng Chem Res, 1996, 35: 1496–1505
4 Bos ANR, Westerterp KR. Mechanism and kinetics of the selective hydrogenation of ethyne and ethene. Chem Eng Processing-Process Intensification, 1993, 32: 1–7
5 Wang B, Yu X, Huo C, *et al.* Density functional theory study of the adsorption and reaction of C_2H_4 on $Fe_3C(100)$. Chin J Catal, 2014, 35: 28–37
6 Armbrüster M, Behrens M, Cinquini F, *et al.* How to control the selectivity of palladium-based catalysts in hydrogenation reactions: The role of subsurface chemistry. ChemCatChem, 2012, 4: 1048–1063
7 Mao S, Zhao B, Wang Z, *et al.* Tuning the catalytic performance for the semi-hydrogenation of alkynols by selectively poisoning the active sites of Pd catalysts. Green Chem, 2019, 21: 4143–4151
8 Luo Q, Wang Z, Chen Y, *et al.* Dynamic modification of palladium catalysts with chain alkylamines for the selective hydrogenation of alkynes. ACS Appl Mater Interfaces, 2021, 13: 31775–31784
9 Wang Z, Luo Q, Mao S, *et al.* Fundamental aspects of alkyne semi-hydrogenation over heterogeneous catalysts. Nano Res, 2022, 15: 10044–10062
10 Qiao B, Wang A, Yang X, *et al.* Single-atom catalysis of CO oxidation using Pt_1/FeO_x. Nat Chem, 2011, 3: 634–641
11 Yang XF, Wang A, Qiao B, *et al.* Single-atom catalysts: A new frontier in heterogeneous catalysis. Acc Chem Res, 2013, 46: 1740–1748
12 Wang A, Li J, Zhang T. Heterogeneous single-atom catalysis. Nat Rev

Chem, 2018, 2: 65–81
13 Liu JC, Tang Y, Wang YG, *et al.* Theoretical understanding of the stability of single-atom catalysts. Natl Sci Rev, 2018, 5: 638–641
14 Kyriakou G, Boucher MB, Jewell AD, *et al.* Isolated metal atom geometries as a strategy for selective heterogeneous hydrogenations. Science, 2012, 335: 1209–1212
15 Liu P, Zhao Y, Qin R, *et al.* Photochemical route for synthesizing atomically dispersed palladium catalysts. Science, 2016, 352: 797–800
16 Yan H, Cheng H, Yi H, *et al.* Single-atom Pd_1/graphene catalyst achieved by atomic layer deposition: Remarkable performance in selective hydrogenation of 1,3-butadiene. J Am Chem Soc, 2015, 137: 10484–10487
17 Hu M, Zhao S, Liu S, *et al.* MOF-confined sub-2 nm atomically ordered intermetallic PdZn nanoparticles as high-performance catalysts for selective hydrogenation of acetylene. Adv Mater, 2018, 30: 1801878
18 Thomas JM. Tens of thousands of atoms replaced by one. Nature, 2015, 525: 325–326
19 Feng Q, Zhao S, Xu Q, *et al.* Mesoporous nitrogen-doped carbon-nanosphere-supported isolated single-atom Pd catalyst for highly efficient semihydrogenation of acetylene. Adv Mater, 2019, 31: 1901024
20 Vilé G, Albani D, Nachtegaal M, *et al.* A stable single-site palladium catalyst for hydrogenations. Angew Chem Int Ed, 2015, 54: 11265–11269
21 Ji S, Chen Y, Zhao S, *et al.* Atomically dispersed ruthenium species inside metal-organic frameworks: Combining the high activity of atomic sites and the molecular sieving effect of MOFs. Angew Chem Int Ed, 2019, 58: 4271–4275
22 Yang F, Ding S, Song H, *et al.* Single-atom Pd dispersed on nanoscale anatase TiO_2 for the selective hydrogenation of phenylacetylene. Sci China Mater, 2020, 63: 982–992
23 Qiao B, Liu J, Wang YG, *et al.* Highly efficient catalysis of preferential oxidation of CO in H_2-rich stream by gold single-atom catalysts. ACS Catal, 2015, 5: 6249–6254
24 Qiao B, Liang JX, Wang A, *et al.* Ultrastable single-atom gold catalysts with strong covalent metal-support interaction (CMSI). Nano Res, 2015, 8: 2913–2924
25 Liang JX, Yang XF, Wang A, *et al.* Theoretical investigations of non-noble metal single-atom catalysis: Ni_1/FeO_x for CO oxidation. Catal Sci Technol, 2016, 6: 6886–6892
26 Tang Y, Wang YG, Li J. Theoretical investigations of $Pt_1@CeO_2$ single-atom catalyst for CO oxidation. J Phys Chem C, 2017, 121: 11281–11289
27 Zhao S, Chen F, Duan S, *et al.* Remarkable active-site dependent H_2O promoting effect in CO oxidation. Nat Commun, 2019, 10: 3824
28 Kistler JD, Chotigkrai N, Xu P, *et al.* A single-site platinum CO oxidation catalyst in zeolite KLTL: Microscopic and spectroscopic determination of the locations of the platinum atoms. Angew Chem Int Ed, 2014, 53: 8904–8907
29 Li T, Liu F, Tang Y, *et al.* Maximizing the number of interfacial sites in single-atom catalysts for the highly selective, solvent-free oxidation of primary alcohols. Angew Chem Int Ed, 2018, 57: 7795–7799
30 Yang M, Li S, Wang Y, *et al.* Catalytically active Au-$O(OH)_x$-species stabilized by alkali ions on zeolites and mesoporous oxides. Science, 2014, 346: 1498–1501
31 Flytzani-Stephanopoulos M. Gold atoms stabilized on various supports catalyze the water-gas shift reaction. Acc Chem Res, 2014, 47: 783–792
32 Lin J, Wang A, Qiao B, *et al.* Remarkable performance of Ir_1/FeO_x single-atom catalyst in water gas shift reaction. J Am Chem Soc, 2013, 135: 15314–15317
33 Tang Y, Wang YG, Liang JX, *et al.* Investigation of water adsorption and dissociation on Au_1/CeO_2 single-atom catalysts using density functional theory. Chin J Catal, 2017, 38: 1558–1565
34 Zhou H, Yang X, Li L, *et al.* PdZn intermetallic nanostructure with Pd-Zn-Pd ensembles for highly active and chemoselective semi-hydrogenation of acetylene. ACS Catal, 2016, 6: 1054–1061
35 Feng Q, Zhao S, Wang Y, *et al.* Isolated single-atom Pd sites in intermetallic nanostructures: High catalytic selectivity for semihydrogenation of alkynes. J Am Chem Soc, 2017, 139: 7294–7301
36 Pei GX, Liu XY, Wang A, *et al.* Ag alloyed Pd single-atom catalysts for efficient selective hydrogenation of acetylene to ethylene in excess ethylene. ACS Catal, 2015, 5: 3717–3725
37 Pei GX, Liu XY, Wang A, *et al.* Promotional effect of Pd single atoms on Au nanoparticles supported on silica for the selective hydrogenation of acetylene in excess ethylene. New J Chem, 2014, 38: 2043–2051
38 Lucci FR, Liu J, Marcinkowski MD, *et al.* Selective hydrogenation of 1,3-butadiene on platinum-copper alloys at the single-atom limit. Nat Commun, 2015, 6: 8550
39 Zhang S, Nguyen L, Liang JX, *et al.* Catalysis on singly dispersed bimetallic sites. Nat Commun, 2015, 6: 7938
40 Ma XL, Liu JC, Xiao H, *et al.* Surface single-cluster catalyst for N_2-to-NH_3 thermal conversion. J Am Chem Soc, 2018, 140: 46–49
41 Ma XL, Yang Y, Xu LM, *et al.* Theoretical investigation on hydrogenation of dinitrogen triggered by singly dispersed bimetallic sites. J Mater Chem A, 2022, 10: 6146–6152
42 Liu JC, Ma XL, Li Y, *et al.* Heterogeneous Fe_3 single-cluster catalyst for ammonia synthesis *via* an associative mechanism. Nat Commun, 2018, 9: 1610
43 Xing DH, Xu CQ, Wang YG, *et al.* Heterogeneous single-cluster catalysts for selective semihydrogenation of acetylene with graphdiyne-supported triatomic clusters. J Phys Chem C, 2019, 123: 10494–10500
44 Liu JC, Xiao H, Zhao XK, *et al.* A novel series of single-cluster catalysts: Transition metal trimer clusters supported on graphdiyne. ChemRxiv, 2020, 1–22
45 Chen JC, Cao H, Chen JW, *et al.* Heterogeneous two-atom single-cluster catalysts for the nitrogen electroreduction reaction. J Phys Chem C, 2021, 125: 19821–19830
46 Liu JC, Xiao H, Zhao XK, *et al.* Computational prediction of graphdiyne-supported three-atom single-cluster catalysts. CCS Chem, 2023, 5: 152–163
47 Guo Y, Yu X, Yu Q, *et al.* Exploring stability of transition-metal single atoms on Cu_2O surfaces. J Phys Chem C, 2022, 126: 8065–8078
48 Chen B, Jiang YF, Xiao H, *et al.* Bimetallic single-cluster catalysts anchored on graphdiyne for alkaline hydrogen evolution reaction. Chin J Catal, 2023, 50: 306–313
49 Talib SH, Hussain S, Baskaran S, *et al.* Chromium single-atom catalyst with graphyne support: A theoretical study of NO oxidation and reduction. ACS Catal, 2020, 10: 11951–11961
50 Kim WJ, Moon SH. Modified Pd catalysts for the selective hydrogenation of acetylene. Catal Today, 2012, 185: 2–16
51 Li Y, Xu B, Fan Y, *et al.* The effect of titania polymorph on the strong metal-support interaction of Pd/TiO_2 catalysts and their application in the liquid phase selective hydrogenation of long chain alkadienes. J Mol Catal A-Chem, 2004, 216: 107–114
52 Kim W. Effect of potassium addition on the properties of a TiO_2-modified Pd catalyst for the selective hydrogenation of acetylene. Appl Catal A-Gen, 2004, 268: 77–82
53 Panpranot J, Kontapakdee K, Praserthdam P. Effect of TiO_2 crystalline phase composition on the physicochemical and catalytic properties of Pd/TiO_2 in selective acetylene hydrogenation. J Phys Chem B, 2006, 110: 8019–8024
54 Yang J, Lv CQ, Guo Y, *et al.* A DFT + U study of acetylene selective hydrogenation on oxygen defective anatase (101) and rutile (110) TiO_2 supported Pd_4 cluster. J Chem Phys, 2012, 136: 104107
55 Liu P, Zhao Y, Qin R, *et al.* A vicinal effect for promoting catalysis of Pd_1/TiO_2: Supports of atomically dispersed catalysts play more roles than simply serving as ligands. Sci Bull, 2018, 63: 675–682
56 Ge X, Zhou P, Zhang Q, *et al.* Palladium single atoms on TiO_2 as a photocatalytic sensing platform for analyzing the organophosphorus pesticide chlorpyrifos. Angew Chem Int Ed, 2020, 59: 232–236
57 Kresse G, Furthmüller J. Efficiency of *ab-initio* total energy calculations for metals and semiconductors using a plane-wave basis set. Comput Mater Sci, 1996, 6: 15–50
58 Kresse G, Furthmüller J. Efficient iterative schemes for *ab initio* total-energy calculations using a plane-wave basis set. Phys Rev B, 1996, 54: 11169–11186
59 Blöchl PE. Projector augmented-wave method. Phys Rev B, 1994, 50: 17953–17979
60 Kresse G, Joubert D. From ultrasoft pseudopotentials to the projector

augmented-wave method. Phys Rev B, 1999, 59: 1758–1775
61 Perdew JP, Burke K, Ernzerhof M. Generalized gradient approximation made simple. Phys Rev Lett, 1996, 77: 3865–3868
62 Tang Y, Zhao S, Long B, *et al.* On the nature of support effects of metal dioxides MO_2 (M = Ti, Zr, Hf, Ce, Th) in single-atom gold catalysts: Importance of quantum primogenic effect. J Phys Chem C, 2016, 120: 17514–17526
63 Heyden A, Bell AT, Keil FJ. Efficient methods for finding transition states in chemical reactions: Comparison of improved dimer method and partitioned rational function optimization method. J Chem Phys, 2005, 123: 224101
64 Henkelman G, Uberuaga BP, Jónsson H. A climbing image nudged elastic band method for finding saddle points and minimum energy paths. J Chem Phys, 2000, 113: 9901–9904
65 Henkelman G, Jónsson H. Improved tangent estimate in the nudged elastic band method for finding minimum energy paths and saddle points. J Chem Phys, 2000, 113: 9978–9985
66 Tang W, Sanville E, Henkelman G. A grid-based Bader analysis algorithm without lattice bias. J Phys-Condens Matter, 2009, 21: 084204
67 Bader RFW. A quantum theory of molecular structure and its applications. Chem Rev, 1991, 91: 893–928
68 Deringer VL, Tchougréeff AL, Dronskowski R. Crystal orbital hamilton population (COHP) analysis as projected from plane-wave basis sets. J Phys Chem A, 2011, 115: 5461–5466
69 Dronskowski R, Bloechl PE. Crystal orbital Hamilton populations (COHP): Energy-resolved visualization of chemical bonding in solids based on density-functional calculations. J Phys Chem, 1993, 97: 8617–8624
70 Burdett JK, Hughbanks T, Miller GJ, *et al.* Structural-electronic relationships in inorganic solids: Powder neutron diffraction studies of the rutile and anatase polymorphs of titanium dioxide at 15 and 295 K. J Am Chem Soc, 1987, 109: 3639–3646
71 Diebold U. The surface science of titanium dioxide. Surf Sci Rep, 2003, 48: 53–229
72 Lee BH, Park S, Kim M, *et al.* Reversible and cooperative photoactivation of single-atom Cu/TiO_2 photocatalysts. Nat Mater, 2019, 18: 620–626
73 Wan J, Chen W, Jia C, *et al.* Defect effects on TiO_2 nanosheets: Stabilizing single atomic site Au and promoting catalytic properties. Adv Mater, 2018, 30: 1705369
74 Ji S, Chen Y, Wang X, *et al.* Chemical synthesis of single atomic site catalysts. Chem Rev, 2020, 120: 11900–11955
75 Fujiwara K, Pratsinis SE. Single Pd atoms on TiO_2 dominate photocatalytic NO_x removal. Appl Catal B-Environ, 2018, 226: 127–134
76 Zhang J, Zhang M, Han Y, *et al.* Nucleation and growth of palladium clusters on anatase TiO_2 (101) surface: A first principle study. J Phys Chem C, 2008, 112: 19506–19515
77 Liu JC, Xiao H, Li J. Constructing high-loading single-atom/cluster catalysts *via* an electrochemical potential window strategy. J Am Chem Soc, 2020, 142: 3375–3383
78 Yang B, Burch R, Hardacre C, *et al.* Origin of the increase of activity and selectivity of nickel doped by Au, Ag, and Cu for acetylene hydrogenation. ACS Catal, 2012, 2: 1027–1032
79 Meng LD, Wang GC. A DFT + U study of acetylene selective hydrogenation over anatase supported Pd_aAg_b ($a + b = 4$) cluster. Phys Chem Chem Phys, 2014, 16: 17541–17550
80 Hammer B, Norskov JK. Why gold is the noblest of all the metals. Nature, 1995, 376: 238–240
81 Kozuch S, Martin JML. What makes for a bad catalytic cycle? A theoretical study on the Suzuki–Miyaura reaction within the energetic span model. ACS Catal, 2011, 1: 246–253
82 Kozuch S, Martin JML. What makes for a good catalytic cycle? A theoretical study of the SPhos ligand in the Suzuki–Miyaura reaction. Chem Commun, 2011, 47: 4935–4937
83 Kozuch S, Shaik S. How to conceptualize catalytic cycles? The energetic span model. Acc Chem Res, 2011, 44: 101–110

Acknowledgements This work was supported by the Foundation of Key Laboratory of Low-Carbon Conversion Science & Engineering, Shanghai Advanced Research Institute, Chinese Academy of Sciences (KLLCCSE-201902, SARI, CAS), the National Natural Science Foundation of China (22033005, 22002004, 22273053 and 92261203), the National Key R&D Project (2022YFA1503900 and 2022YFA1503000), the NSFC Center for Single-Atom Catalysis, and the Natural Science Basic Research Program of Shaanxi (S2020-JC-WT-0001 and S2021JCW-20). Support of Guangdong Provincial Key Laboratory of Catalysis (2020B121201002) is also acknowledged. The calculations were performed by using supercomputers at Tsinghua National Laboratory for Information Science and Technology and by the Center for Computational Science and Engineering at SUSTech.

Author contributions Li J supervised the project. Zhao S conceived the original concept, designed the experiments, and wrote the manuscript. Tang Y provided helpful discussion during the revision process. Yu X and Li J revised the manuscript, and all authors contributed to the general discussion.

Conflict of interest The authors declare that they have no conflict of interest.

Supplementary information Supporting data are available in the online version of the paper.

Shu Zhao received her BSc degree (applied chemistry, in 2009) at Inner Mongolia University and PhD degree (physical chemistry, in 2015) at Chinese Academy of Sciences. In 2015, she began to work at Tsinghua University with professor Jun Li as a post-doctoral fellow. Two years later, she joined the faculty at Beijing University of Technology as a lecturer. Her main research interest is computational investigation and design of advanced materials for energy storage and conversion.

Yan Tang received her BSc degree from the School of Chemistry and Molecular Engineering, East China University of Science and Technology (ECUST) in 2014 and her PhD degree from Tsinghua University in 2019. Her PhD research focuses on the theoretical investigations on single atom catalysts (SACs).

Xiaohu Yu received his PhD degree from the Institute of Coal Chemistry, Chinese Academy of Sciences in 2013. He did postdoctoral research at Moscow Institute of Physics and Technology from 2013 to 2015. He worked as a visiting scholar in Prof. Jun Li's group at Tsinghua University from 2019 to 2020. He is now a full professor at Shaanxi University of Technology. His research interests focus on theoretical inorganic chemistry and computational catalysis science.

Jun Li received his PhD degree from Fujian Institute of Research on the Structure of Matter, Chinese Academy of Sciences in 1992. He did postdoctoral research at the University of Siegen and The Ohio State University from 1994 to 1997. He worked as a research scientist at The Ohio State University as well as Senior Research Scientist and Chief Scientist at the Pacific Northwest National Laboratory from 1997 to 2009. He is now a ChangJiang Chair Professor at Tsinghua University. His research involves quantum theoretical chemistry, heavy-element chemistry, and computational catalysis science.

单团簇催化剂在乙炔半加氢反应中的优异反应性

赵妹[1,2], 汤妍[3], 于小虎[4*], 李隽[3,5*]

摘要 载体上孤立的Pd原子作为乙炔半加氢反应的催化活性位点，由于具有独特的反应性和高效的金属利用率而备受关注. 特别是在金属氧化物表面的不同位点掺杂Pd单原子，可以通过调节其局部配位环境来调控其电子和催化性能. 本文采用密度泛函理论计算，研究了TiO_2负载Pd单原子的局域配位环境对Pd_1/TiO_2催化剂上乙炔半加氢反应的活性和选择性的影响. 综合考虑反应活性和选择性，发现具有负电荷$Pd^{\delta-}$位点的Pd_1Ti_3/TiO_2四原子单团簇催化剂展现出优异的催化性能. 此外，活性和选择性与表面性质如d-带中心指数和表面功函数等密切相关. 本文为未来设计可还原氧化物载体上的高效单团簇催化剂以用于类似的多相催化反应提供了理论参考.